Talanta 129 (2014) 155–164

Contents lists available at ScienceDirect

Talanta

journal homepage: www.elsevier.com/locate/talanta

A separation of tyramine on a 2-(4-methoxyphenyl)ethylamine imprinted polymer: An answer from theoretical and experimental studies

Piotr Luliński, Monika Sobiech, Teresa Żołek, Dorota Maciejewska *

Department of Organic Chemistry, Faculty of Pharmacy, Medical University of Warsaw, Banacha 1, 02-097 Warsaw, Poland

ARTICLE INFO

Article history:
Received 8 January 2014
Received in revised form
12 May 2014
Accepted 18 May 2014
Available online 24 May 2014

Keywords:
Molecularly imprinted polymers
Tyramine
Molecular modeling
Solid phase extraction

ABSTRACT

A 2-(4-methoxyphenyl)ethylamine imprinted polymer (MIP) was successfully applied for the selective separation of tyramine. A computational analysis was used to predict the affinity of the polymer matrix towards tyramine and a preliminary experimental evaluation was made for the target analyte. Then the experimental analysis of polymer towards tyramine was continued. The binding sites were characterized with employment of the Langmuir and Freudlich models. After the optimization of solid phase extraction towards tyramine, the most appropriate systems for the extraction steps were chosen: methanol–water 85:15 v/v for the loading and the washing as well as 0.04 M aq. ammonium acetate–methanol 30:70 v/v for the elution steps. The biogenic compounds as tryptamine, serotonin, octopamine, synephrine, and L-tyrosine were used for the selectivity study on the basis of binding capacities of the analytes on the imprinted and the non-imprinted polymers. The theoretical approach to obtained results allowed to explain the adsorption selectivity of the tested polymer. Finally, the complex matrix of bovine serum albumin was used to show the usefulness of imprinted material for bioanalysis. The obtained recoveries showed the superiority of MIP over the commercial sorbent C18. Total recoveries of tyramine from spiked bovine serum albumin sample were determined as: $95 \pm 2\%$, $14 \pm 3\%$, and $1.9 \pm 0.4\%$ for the imprinted, non-imprinted, and commercial C18 sorbents, respectively.

1. Introduction

Tyramine (2-(4-hydroxyphenyl)ethylamine) is the most important trace biogenic amine synthesized in the mammalian brain and the peripheral nervous tissues. Trace biogenic amines are metabolically associated with dopamine, norepinephrine, and serotonin neurotransmitter systems and they are implicated in a vast array of human disorders related to mood, emotion, attention and cognition [1]. Tyramine acts as the biosynthetic intermediate precursor of octopamine [2] and is a product of tyrosine metabolism after the activation of tyrosine decarboxylase [3]. Recently, new tyramine receptors were discovered. This fact promoted extensive studies which suggest that tyramine may comprise its own independent neurotransmitter system [4,5].

Tyramine is present in the mammalian brain in a very low concentration in the range of 0.1–100 ng g^{-1} of tissue [1,6]. The intracorporeal concentration of tyramine may increase after the consumption of tyramine rich food (cheese is such diary product where tyramine is produced after the decarboxylation of tyrosine promoted by bacteria species) [7,8]. In the mammalian organism detoxification mechanism involves monoaminooxidase system to metabolize tyramine. This process can be insufficient during inappropriate diet and consumption of antidepressant or antitubercular drugs [7,9]. As a potent vasoconstrictor, tyramine can induce a hypertensive crisis, severe headache, intracranial hemorrhage, neuronal sequelae, cardiac failure and pulmonary edema [10,11]. Hence, the determination of tyramine is a very important scientific goal from biomedical and dietary points of view. The analytical methods as GC or HPLC coupled with mass spectrometry, capillary zone electrophoresis or quantitative polymerase chain reaction are also employed in the determination of tyramine [11–13] with good selectivity and detection limits, but they required the pretreatment steps (for example: derivatization) and the expensive instruments. The accuracy in determination of tyramine is hampered by the complexity of sample matrix. Hence, the extraction and clean-up steps are necessary before the analysis [14]. The solid phase extraction (SPE) improved the recoveries from extracts and allows for the determination of the target analytes that occur in trace amounts. Nevertheless, commercial SPE sorbents retain the analytes by non-selective hydrophobic or polar interactions which lead to the coextraction of interfering compounds. The lack of selective sorbents is the major limitation

* Corresponding author. Tel./fax: +48 22 5720643.
E-mail address: dorota.maciejewska@wum.edu.pl (D. Maciejewska).

http://dx.doi.org/10.1016/j.talanta.2014.05.029
0039-9140/

of SPE. Among the promising methods used for selective separation is the molecularly imprinted solid phase extraction (MISPE) [15], where the molecularly imprinted polymers that are produced by the imprinting technique provide the stationary phase with the desired selectivity [16].

Until now, there are only a few papers related to produce of tyramine imprinted materials. Huang and co-workers [17] developed a novel sensitive imprinted electrochemical sensor for determination of tyramine. The sensor was produced combining multiwalled carbon nanotubes–gold particles composites, chitosan and imprinted film. The molecularly imprinted layer was synthesized using tyramine as a template and tetraethylorthosilicate and triethoxyphenylsilane as the functional monomers. The composite material enhanced the sensitivity (limit of detection for tyramine was 58 nmol L^{-1}) and the imprinted layer provided high selectivity (low response for dopamine, tyrosine and L-DOPA). The determination of tyramine from the diary samples showed good recovery (92.1–109.3%). Atta and co-workers [18,19] obtained the electrochemical sensors based on tetraethylorthosilicate and phenyltriethylorthosilicate as the functional monomers for the detection of tyramine and dopamine. Selectivity studies revealed that dopamine was partially adsorbed on the tyramine imprinted surface.

Our group is engaged in searching for new selective materials for separation of neurotransmitters and their metabolites, which could improve their detection and finally could help to explain some aspects of pathoneurological diseases [20–23]. Previously, we described the synthesis and the characteristics of the 2-(4-methoxyphenyl)ethylamine imprinted polymer (MIP) [23]. We concluded that this polymer has a potential as the selective sorbent for the isolation of bioamines. This inspired us to check theoretically such possibility, and in this paper we created the theoretical model of the polymer cavity [24] in the MIP prepared from methacrylic acid in toluene. Then, this model was used for evaluation of the polymer affinity towards tyramine **(1)** and the selected biogenic compounds. We found that this polymer could be very efficient sorbent for the selective separation of **(1)**. This hypothesis was proved experimentally by SPE of **(1)** on the MIP which was *de novo* synthesized [23]. The binding sites of obtained polymer and its non-imprinted counterpart (NIP) were characterized for adsorption of (**1**) using the Langmuir and Freudlich models. The theoretical analysis of the intermolecular interactions in the polymer cavity was used to explain the polymer matrix selectivity towards the biogenic compounds as tryptamine (**2**), serotonin (**3**), octopamine (**4**), synephrine (**5**), and L-tyrosine (**6**). Finally, the optimized SPE protocol for the separation of (**1**) was used in the determination of (**1**) in the model sample matrix and compared with the results obtained on the commercial C18 sorbent.

2. Materials and methods

2.1. Experimental examinations

2.1.1. Materials

2-(4-Methoxyphenyl)ethylamine, (**T**) was purchased from Fluka (Steinheim, Germany). Tyramine, 4-(2-aminoethyl)phenol hydrochloride (**1**); tryptamine, 2-(3-indolyl)ethylamine (**2**); serotonin, 3-(2-aminoethyl)-5-hydroxyindole hydrochloride **(3)**; *R*/*S*-octopamine, 1-(4-hydroxyphenyl)-2-aminoethanol hydrochloride (**4**); *R*/*S*-synephrine, 1-(4-hydroxyphenyl)-2-methylaminoethanol (**5**); and L-tyrosine, *S*-2-amino-3-(4-hydroxyphenyl)propionic acid (**6**) were from Sigma-Aldrich (Steinheim, Germany). The functional monomer, methacrylic acid, and the cross-linker, ethylene glycol dimethacrylate were from Fluka (Steinheim, Germany). The polymerization reaction initiator, 2,2′-azobisisobutylocarbonitrile, was from Merck (Darmstadt, Germany). The solvents used in synthesis and analysis: toluene, methanol, isopropanol, acetonitrile, acetone, were from POCh (Gliwice, Poland), and formamide was from Fluka (Buchs, Switzerland). Methanol (analytical grade) was provided by POCh (Gliwice, Poland). Ammonium acetate was from POCh (Gliwice, Poland). The monomers were purified prior to use by vacuum distillation. All other reagents were used without further purification. Ultra-pure water delivered from a Milli-Q purification system (Millipore, France) was used to prepare the water solutions.

Bovine serum albumin was delivered from Serva (Heidelberg, Germany). The commercial C18 stationary phase was from J.T. Baker (Phillipsburg, NJ, USA).

2.1.2. Instruments and calibration lines

The stock solutions of the compounds (**1**)–(**6**) were prepared by accurate weighting the appropriate amount of each compound and dissolving it in methanol for (**1**)–(**5**) or in 0.1 M aq. HCl for **(6)** to obtain the concentration of 10 mmol L^{-1}. The standard solutions were prepared prior to use by dilution of the appropriate stock solutions with methanol–water 85:15 v/v, and for (**1**) additionally with methanol, methanol–water 50:50 v/v, methanol–water 15:85 v/v, and water to obtain the required concentrations. All stock solutions were stored in the dark at +8 °C.

The UV measurements were performed with a UV-1605PC spectrophotometer (Shimadzu, Germany). The calibration lines were constructed as a function of peak area under absorbance curve at λ_{max} of each compound (y) versus concentration (x). Each point was measured in triplicate. The linearity of calibration lines was good with correlation coefficients $r^2 > 0.997$. The wavelength, λ_{max}, the limits of quantification, LOQ (in μmol L^{-1}) and the limits of detection, LOD (in μmol L^{-1}) were as follows: **(1)**, 277, 16.26, 5.36; **(2)**, 280, 4.43, 1.46; **(3)**, 276, 19.40, 6.40; **(4)**, 275, 12.78, 4.22; **(5)**, 276, 21.31, 7.03; **(6)**, 276, 21.53, 7.11.

RP-HPLC was used for the determination of (**1**) in bovine serum albumin. The HPLC system consisted of a LC 10AT pump, an CTO 10A oven, a RF 551 spectrofluorimetric detector operated at λ_{ex}=280 nm and λ_{em}=315 nm, and an SIL 20A HT autosampler (Shimadzu, Germany). Chromatographic separation was performed using a Discovery HS F5 stainless steel column (150 mm × 4.6 mm ID, 5 μm, Supelco, Bellefonte, PA, USA), preceded by a 20 mm × 4.6 mm ID, Discovery HS F5 guard column. The mobile phase consisted of 0.05 M aq. pH 3 ammonium formate–methanol 5:95 v/v delivered at a flow rate of 1 mL min^{-1}. The five-point calibration line was constructed as a function of peak area (x) versus concentration (y) in the range of 2.5–50 μmol L^{-1}. The linearity of calibration line was good with the correlation coefficients $r^2 > 0.998$, LOQ and LOD values (in μmol L^{-1}) were 2.29 and 0.76, respectively.

2.1.3. Preparation of polymers

The MIP was prepared as a bulk material accordingly to the recipe shown in the previous paper [23]. The template removal was carried out in SPE cartridges with 0.04 M aq. ammonium acetate – methanol 30:70 v/v system and was controlled by UV spectroscopy. Non-imprinted polymer (NIP) was prepared under the same polymerization conditions but without the template molecule and was treated in the same way as the corresponding imprinted polymer.

2.1.4. Characterization of binding sites

The stationary binding experiments were carried out for characterization of binding sites (the Langmuir and Freudlich models). Polypropylene tubes were filled with 20 mg of MIP or NIP particles. Next, a volume of 5 mL of the standard solutions of (**1**) were added (concentrations: 10–300 μmol L^{-1}). The tubes

were sealed and oscillated by a shaker (Heidolph, Germany) at room temperature for 24 h. Then the tubes were centrifuged for 10 min at 3000 rpm and the aliquots of supernatant (0.7 mL) were used to analyze the unbound amount of (**1**) using the calibration line. The amount of (**1**) bound to the polymer was calculated by subtracting the unbound amount from the initial amount of (**1**).

2.1.5. Optimization of SPE procedure

2.1.5.1. Optimization of loading step. The dynamic procedure was performed to evaluate the loading capacity of the particles. Polypropylene SPE columns (Chromabond, Germany) of 1 mL were filled with 25 mg of MIP or NIP particles and secured by glass-fiber frits. The particles were conditioned with appropriate solvent (1 mL, methanol, methanol–water 85:15 v/v, methanol–water 50:50 v/v, methanol–water 15:85 v/v or water) and then the standard solution of (**1**) (50 μmol L^{-1}) was loaded (until adsorption on the polymer was not observed) with successive portions of 2 mL. The flow rate was 1 mL min^{-1}. The aliquots of supernatant (0.7 mL) were used to analyze the unbound amount of (**1**) using the calibration line. The bound amount of (**1**) was calculated by subtracting the unbound amount from the initial amount of (**1**).

2.1.5.2. Optimization of washing step. In the washing optimization, the procedure was performed as described above with conditioning and loading of the standard solution (**1**) with the successive portions of 2 mL (methanol–water, 85:15 v/v, 50 μmol L^{-1}). The amount of (**1**) adsorbed on the particles was calculated as described above. Only on NIP, the 2 mL of washing solvent, *viz.* acetonitrile, isopropanol, water or formamide–water 2:98 v/v were applied, and on both, MIP and NIP, 2 mL of washing solvent, *viz.* methanol, methanol–water 85:15 v/v, formamide–methanol 10:90 v/v or formamide–water 10:90 v/v were applied. Finally, the successive steps of 2 mL of eluent (0.04 M aq. ammonium acetate–methanol 30:70 v/v) were applied to desorb tyramine and the aliquot of eluate of 0.7 mL was used to analyze the amount of (**1**) desorbed either from MIP and NIP.

2.1.5.3. Optimization of elution step. In the elution optimization varied eluents were tested, *viz.* 0.2 M aq. ammonium acetate–methanol 30:70 v/v, 0.04 M aq. ammonium acetate–methanol 30:70 v/v, 0.008 M aq. ammonium acetate–methanol 30:70 v/v, 0.04 M aq. ammonium acetate–methanol 50:50 v/v, and methanol. All experiments were carried-out in triplicate.

2.1.5.4. Optimization of solution volume and mass of particles. To optimize the volume of the loaded solutions and the mass of particles, polypropylene 1 mL SPE columns secured by glass-fiber frits were filled with 25 or 50 mg of MIP or NIP particles. All steps of the optimized SPE procedure were applied on each column. The flow rate of each SPE step was 1 mL min^{-1}. The elution fractions were collected and aliquots of 0.7 mL were used to analyze the amount of (**1**) eluted from MIP or NIP. Triplicate cartridges were used for each extraction.

2.1.6. Affinity tests

The affinity studies were performed on MIP or NIP particles for the compounds **(1)–(6)** in the non-competitive binding experiments using the dynamic procedure. Polypropylene SPE columns of 1 mL secured by glass-fiber frits were filled with 50 mg of MIP or NIP particles. The particles were conditioned with methanol–water 85:15 v/v, 1 mL, then loaded with the successive portions of 2 mL (until no further adsorption on polymer was observed) of methanol–water 85:15 v/v standard solution of 20 μmol L^{-1} of each compound (**1**)–(**6**). The flow rate was 1 mL min^{-1}. The fractions were collected and the amounts of the analyte were analyzed using the calibration lines. All experiments were performed in triplicate.

*2.1.7. SPE of tyramine (**1**) from bovine serum albumin*

Bovine serum albumin (25 mg) was transferred to a volumetric flask of 250 mL and dissolved in 37.5 mL of ultra-pure water. The flask was filled-up with methanol, mixed and stored at +8 °C for 3 h. Next, the solution was filtered off and stored at +8 °C for further analysis.

SPE experiments were carried out on a Macherey–Nagel SPE manifold. Polypropylene 1 mL SPE columns secured by glass-fiber frits were filled with a 50 mg of MIP, NIP or C18. The optimized SPE protocol was used in testing. The loading step consists of 5 mL of bovine serum albumin solution spiked with **(1)** (concentration of 52.3 μmol L^{-1}). The concentration of (**1**) in eluate was determined by HPLC method using spectrofluorometric detection. The flow rate of each SPE step was 0.5 mL min^{-1}. Triplicate cartridges containing either MIP, NIP or C18 were used for extraction.

2.2. Molecular modeling

The polymer matrix was constructed from the functional monomer – methacrylic acid and the cross-linker – ethylene glycol dimethacrylate surrounding the template: 2-(4-methoxyphenyl)ethylamine (**T**). In the affinity tests the following analytes were used: the target analyte – tyramine (**1**) and the selected biogenic compounds (**2**)–(**6**).

2.2.1. Methodology

In the first step, three-dimensional structures of (**T**), methacrylic acid, ethylene glycol dimethacrylate, and compounds (**1**)–(**6**) were generated using Discovery Studio 3.1 program distributed by Accelrys Software Inc. [25]. The geometries of all compounds were optimized using the density functional theory (DFT) with B3LYP/6-311+G (d,p) hybrid functional implemented in the Gaussian 09 program [26]. The so-called ESP-atomic partial charges on the atoms were computed using the Breneman model [27], reproducing the molecular electrostatic potential. Fig. 1 shows the chemical formulas and the theoretical conformations of the template (**T**), the polymer components and the tested analytes (**1**)–(**6**).

In the second step, the polymerization system was created. To get the starting structure, one (**T**) molecule was surrounded by four monomer molecules and twenty molecules of cross-linker, reflecting the stoichiometry of the synthetic procedure. As the polymerization and the adsorption procedures proceed in the solvents, the effect of solvation on the energy calculations was taken into account. The continuum model [28] was used to evaluate the solvent effect which treats the solvent as a uniform polarizable medium with a dielectric constant of εr_{ij} [29]. The energy optimization of the polymerization complex was made using the dielectric constant value of toluen $\varepsilon = 2.38 r_{ij}$ [30]. Toluen was selected for the cavity modeling because it was used as the porogen in preparation of MIP.

All minimizations of energy were made at the molecular mechanics level (MM) with all energy gradients lower than 0.01 kcal mol^{-1} $Å^{-1}$ using two algorithms: the steepest descent algorithm applied with 100 steps, and then conjugate gradient algorithm applied with 10,000 steps. MM simulations were carried out using the CHARMm force field [31] implemented in the module of Discovery Studio 3.1 software.

In the third step, the polymer cavity was constructed on the basis of the polymerization complex structure. Double bonds in the monomer and the cross-linker molecules were replaced by

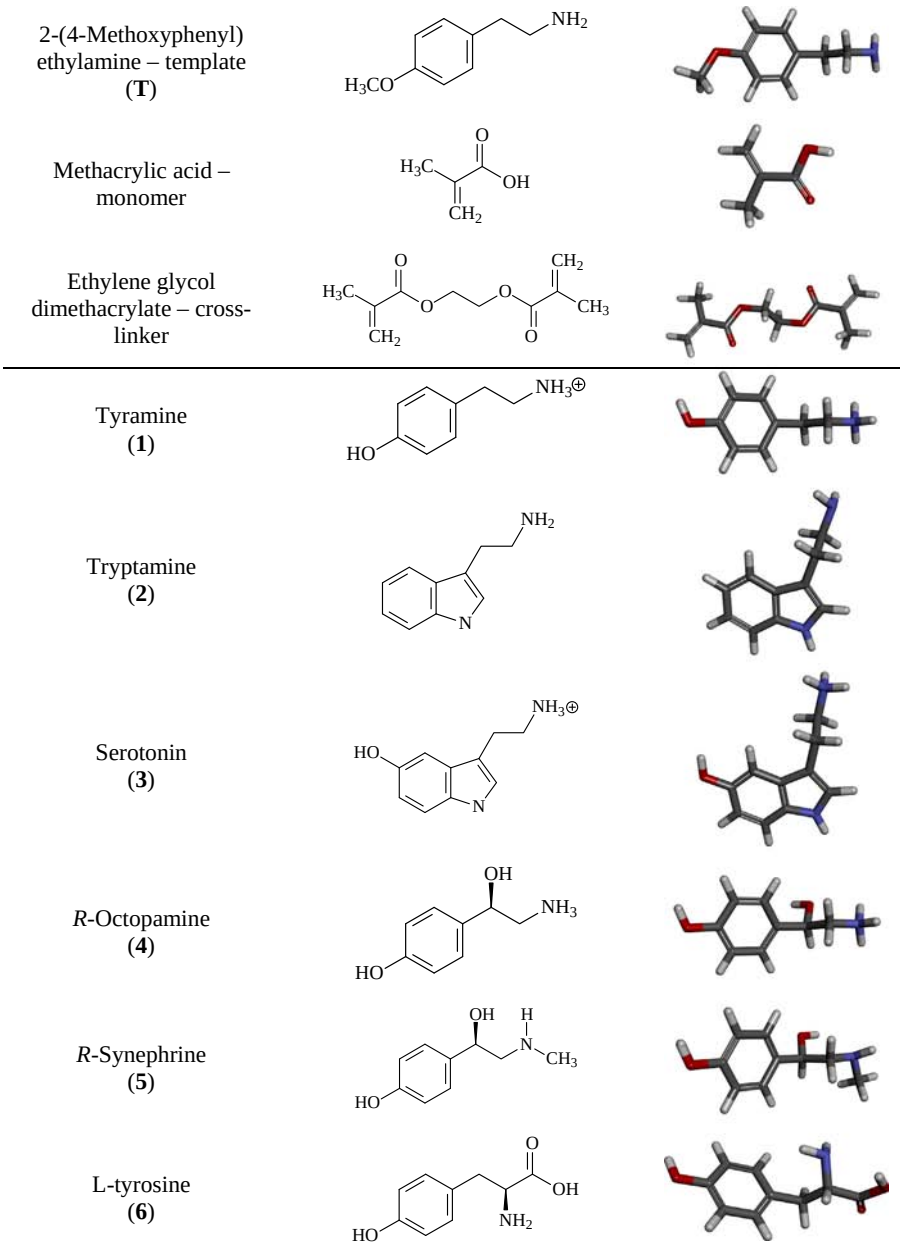

Fig. 1. Chemical formulas and conformations of the template, the monomer, the cross-linker, and the tested compounds.

single bonds (by adding hydrogen to carbon atoms). This operation approximates the formation of single C–C bonds during the polymerization. Next, (**T**) molecule was removed from the complex, and the empty space was proposed as the computer model of the binding site in the polymer matrix.

The cavity was used in the affinity analysis. The tested analytes (**1**)–(**6**) were inserted one by one into the cavity replacing (**T**) molecule, and the energies of complexation as well as the intermolecular interactions were scrutinized.

During the optimization of interactions in the polymer cavity, the constraints were set on the cross-linker and the monomers with force constants of 100 kcal mol^{-1} $Å^{-2}$ in order to immobilize the 3D structure of the cavity. The analytes were left freely, mimicking the adsorption step. The adsorption in the polymer matrix was analyzed applying the MM method using the dielectric constant value of methanol–water 85:15 v/v system $\varepsilon = 36r_{ij}$ [32]. This dielectric constant was used in the adsorption simulation because the methanol–water 85:15 v/v system was used in the binding experiments. The calculation of the binding energies ΔE_B between the analyte and the polymer matrix were performed using Eq. (1):

$$\Delta E_B = E_{system} - E_{analyte} - E_{cavity} \quad (1)$$

where: $E_{analyte}$ – energy of the analyte, E_{cavity} – energy of the polymer cavity (without the analyte), E_{system} – energy of the cavity with bound analyte. MM energies used in calculations were obtained with energy gradients lower than 0.01 kcal mol^{-1} $Å^{-1}$.

3. Results and discussion

3.1. Theoretical model of polymer cavity

According to procedure presented in Section 2.2 we constructed the model of polymer cavity, which composed of four molecules of methacrylic acid and twenty molecules of ethylene

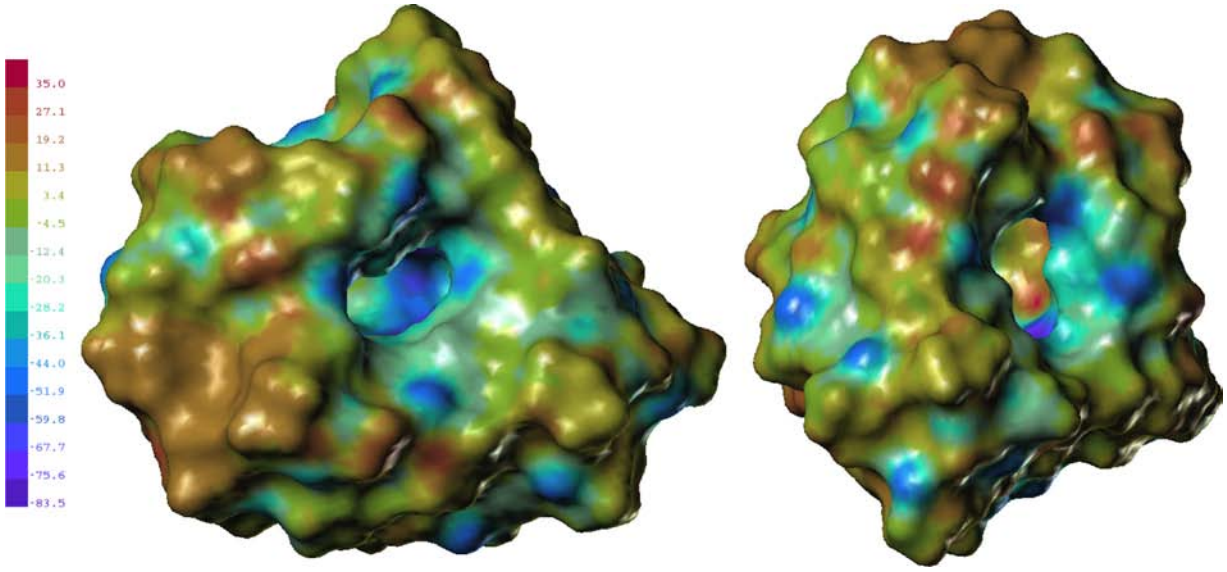

Fig. 2. Two views of the polymer cavity: the surface colored according to molecular electrostatic potential (MEP). Negative values are shown as blue, neutral values – as yellow-green, and positive values – as red-orange. (For interpretation of the references to color in this figure legend, the reader is referred to the web version of this article.)

glycol dimethacrylate. Fig. 2 presents two views of the polymer cavity using molecular electrostatic potential (MEP) which showed the distribution of MEP on the surface of the cavity. Negative values are shown as blue whereas neutral areas as yellow-green, and positive potential values are marked in red-orange. We could observe the regions inside the cavity with the strongly negative and the strongly positive potential. The regions which were closer to the edge at the walls of the cavity had the slightly negative or neutral potential. This means that the electrostatic interactions inside the cavity are much stronger, and the polar analytes can be oriented in specific way.

3.2. Theoretical analysis of MIP affinity towards tyramine (1)

To get insight into the 2-(4-methoxyphenyl)ethylamine imprinted polymer affinity towards **(1)** we have calculated the binding energy ΔE_B of (**T**) and (**1**) in the polymer cavity according to Eq. (1). The strongest interaction with MIP was predicted for T (-31.76 kcal mol^{-1}), but for (**1**) was also very high (-27.87 kcal mol^{-1}). Next, we compared the intermolecular interactions in the polymer cavity for both molecules (**T**) and (**1**). Fig. 3 illustrates the location of (**T**) and (**1**) inside the cavity at the end of the adsorption process. The molecular electrostatic potential was presented on the cavity surface, (**T**) as well as (**1**) were colored according to the partial charge values, and showed next to the cavity for comparison. The hydrogen bonds were presented as the dashed lines. Both compounds had positive charge located on the H atoms of amino groups, and were oriented inside the cavity similarly towards the negative region of electrostatic potential interacting with the functional monomer and the cross-linker. The H atoms of amino groups formed the quite strong hydrogen bonds of the length of 2.06–2.95 Å. Compound (**1**) formed nine hydrogen bonds (eight of them are formed by NH_3^+ group and one by OH group), and (**T**) formed seven hydrogen bonds via amino group. We could suppose that the hydroxyl group of (**1**) provided additional point of anchorage, and enhanced the affinity of polymer towards (**1**).

To testify those findings, MIP was analyzed towards (**1**) by the successive experiments: the characterization of binding sites, the optimization of SPE procedure, and the affinity measurements towards the selected biogenic compounds (**2**)–(**6**).

3.3. Characterization of binding sites

The analysis of binding properties of MIP and NIP towards (**1**) was performed using two models [33]. First the Langmuir model, transformed to the Scatchard equation, Eq. (2) was employed:

$$\frac{B}{F} = \frac{(B_{max} - B)}{K_d} \tag{2}$$

B_{max} is the total number of the binding sites, K_d is the dissociation constant, B is the bound amount of the analyte, and F is the unbound amount of the analyte. The system which fits well to the Langmuir model gives a straight line on Scatchard plot with a slope equal to $-(1/K_d)$ and y-intercept equal to B_{max}/K_d. The system which has more than one kind of binding sites is characterized by more than one line. The binding isotherms were determined by adding a fixed volume of various solutions of (**1**) to a 20 mg of polymers (Section 2.1.4). Scatchard plots for MIP and NIP are presented in Fig. 4.

Two straight lines were observed for MIP and only one for NIP. Two classes of heterogeneous binding sites of MIP are characterized by two K_d and two B_{max} values: $K_d(1) = 9.24$ μmol L^{-1} and $B_{max}(1) = 6.9$ μmol g^{-1} for the higher affinity binding sites, and $K_d(2) = 120$ μmol L^{-1} and $B_{max}(2) = 42.3$ μmol g^{-1} for the lower affinity binding sites. The results showed well that MIP had the selective binding sites complementary to (**1**). NIP had only low affinity binding sites to (**1**) characterized by the value of $K_d = 106$ μmol L^{-1} and $B_{max} = 4.41$ μmol g^{-1}.

Next, the Freundlich model represented by Eq. (3) was used to confirm the surface heterogeneity. That model fits well to MIP adsorption data in the low concentration regions [34].

$$B = aF^m \tag{3}$$

B is the bound amount of the analyte, and F is the unbound amount of the analyte, a is the measure of the capacity (B_{max}) and m is a heterogeneity index. The plots of adsorption employing the Freundlich model is presented in Fig. 5.

The straight line of $\log B$ versus $\log F$ is the evidence that adsorption can be described by the Freudlich equation. The estimated value of m for MIP is 0.69. The result indicated that MIP has a heterogeneous population of binding sites towards (**1**).

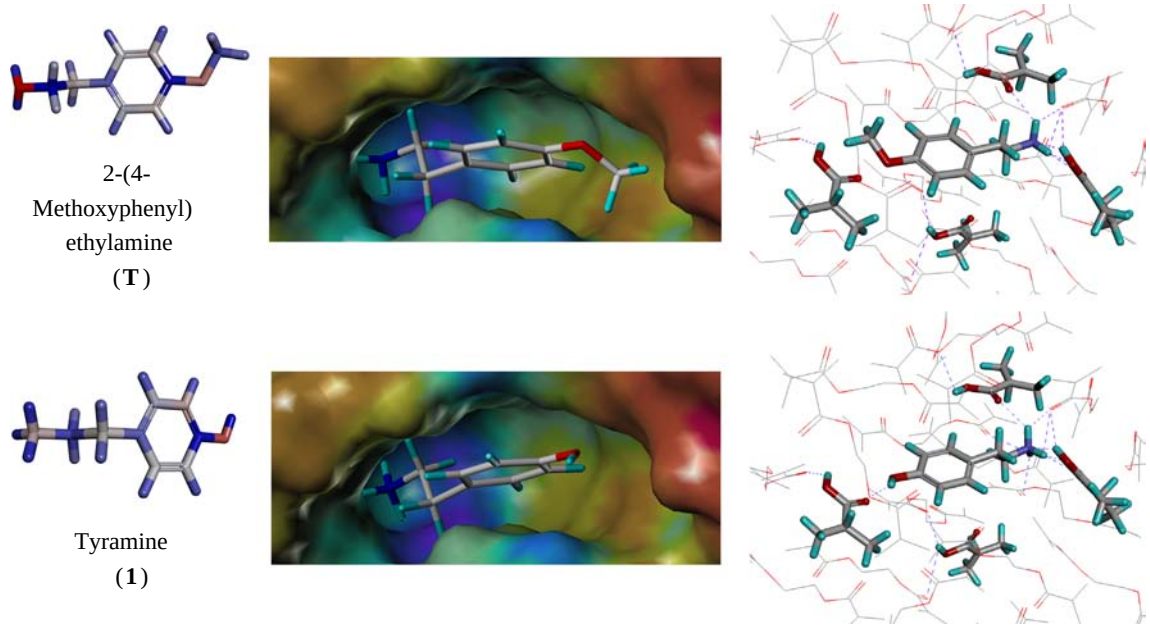

Fig. 3. A view of the template (**T**) and the target analyte (**1**) molecules at the end of the adsorption process. The cavity is colored according to molecular electrostatic potential (MEP). Negative values are shown as blue, neutral values – as yellow-green, and positive values – as red-orange. Compounds (**T**) and (**1**) on the left column are colored according to the partial charge values (negative values are shown as red and -1.0 0.6 positive values as blue). On the right column the hydrogen bonds formed in the polymer cavity are shown as the dashed blue lines. (For interpretation of the references to color in this figure legend, the reader is referred to the web version of this article.)

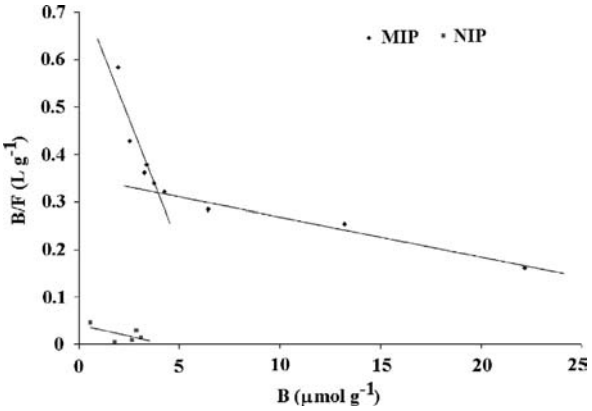

Fig. 4. Scatchard plots of tyramine (**1**) for MIP and NIP: $B/F=f(B)$ where B is the bound amount of the analyte and F is the unbound amount of the analyte.

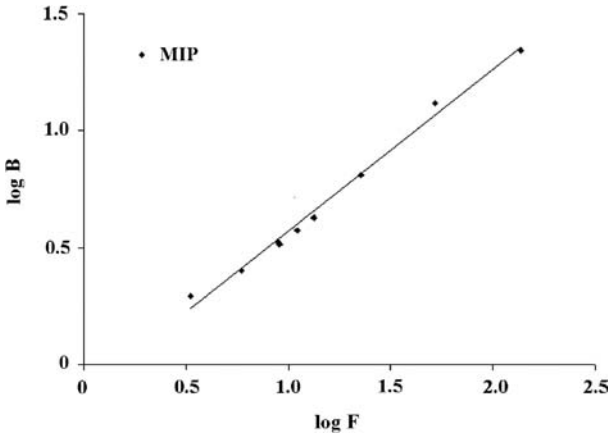

Fig. 5. Freudlich isotherm for tyramine (**1**) for MIP: $B=f(F)$ where B is the bound amount of the analyte and F is the unbound amount of the analyte.

3.4. Optimization of SPE procedure towards tyramine (*1*)

To increase the adsorption of (**1**) on MIP, SPE procedure of (**1**) was optimized.

3.4.1. Optimization of loading step

In order to select the appropriate methanol–water proportion in the solvent for loading step, we determined the binding capacity of MIP and NIP after the loading of the standard solution of (**1**) (50 μmol L^{-1}) on the polymer in the dynamic binding procedure (Section 2.1.5). The binding capacities (B, μmol g^{-1}) of MIP and NIP were calculated according to Eq. (4):

$$B = \sum_{i=1}^{n} \left[\frac{(C_i - C_f)V}{m}\right]_n \quad (4)$$

V represents the volume of portion (mL) in each loading step, n is the number of loading steps performed until further adsorption on the polymer was not observed, C_i represents the initial solution concentration (mmol L^{-1}), C_f represents the solution concentration after adsorption (mmol L^{-1}) and m is the mass of polymer particles.

Next, the binding capacity of MIP and NIP were compared by the determination of affinity factors (AF) calculated according to Eq. (5):

$$AF = \frac{B_{MIP}}{B_{NIP}} \quad (5)$$

Table 1 presents the binding capacity of MIP and NIP and the calculated affinity factors.

The results revealed strong influence of methanol in the aqueous solution of (**1**) on the binding capacity of polymers. The adsorption of (**1**) decreases with increasing percentage of methanol in the loading solution and this trend was more visible on the NIP. This could be

Table 1
Impact of percentage of methanol in aqueous standard solution of tyramine (**1**) on binding capacity of polymer (conc. 50 μmol L^{-1}, $n=3$).

Methanol (%)	Binding capacity ± S.D. (μmol g^{-1})		AF
	MIP	NIP	
100	16.6 ± 0.2	4.3 ± 0.3	3.87
85	16.4 ± 0.2	4.8 ± 0.2	3.46
50	19 ± 2	7.0 ± 0.4	2.71
15	25 ± 2	13 ± 2	1.94
0	27 ± 2	17 ± 1.4	1.58

Table 2
Percentage of tyramine (**1**) eluted from MIP and NIP after applying different washing solvents ($n=3$).

Solvent	Elution recovery of tyramine ± R.S.D. (%)	
	NIP	MIP
Acetonitrile	108 ± 9	–
Water	92 ± 8	–
Isopropanol	57 ± 5	–
Formamide–water 2:98 v/v	52 ± 5	–
Methanol	47 ± 4	95 ± 7
Methanol–water 85:15 v/v	46 ± 4	98 ± 7
Formamide–water 10:90 v/v	31 ± 3	30 ± 3
Formamide–methanol 10:90 v/v	24 ± 2	17 ± 2

explained by the suppression of non-specific binding by methanol. Calculated affinity factors confirmed increase of selectivity with increasing percentage of methanol in solution. Two solvents, *viz*. methanol and methanol–water 85:15 v/v were good candidates as the loading solution for (**1**). Both are characterized by similar binding capacities (16.6 and 16.4 μmol g^{-1}, respectively) and similar affinity factors (3.87 and 3.46, respectively). We decided to use methanol–water 85:15 v/v as the loading solution for further experiments taking into account the solubility of all analytes.

3.4.2. Optimization of washing step

The non-imprinted polymer was prepared in order to analyze the level of non-specific adsorption on the polymer matrix. The cartridges filled with NIP were loaded with the standard solution of **(1)** (50 μmol L^{-1}) and were washed with eight various washing solvents, *viz*. methanol, methanol–water 85:15 v/v, methanol–formamide 10:90 v/v, water, formamide–water 2:98 v/v, formamide–water 10:90 v/v, isopropanol, acetonitrile. After the washing step, the elution with optimized eluent (Section 3.4.3) was proceeded and the recovery of **(1)** (defined as percentage of adsorbed amount) was determined. The results are presented in Table 2 (middle column).

The results revealed substantial influence of the nature of selected solvents on the reduction of non-specific adsorption of (**1**) on NIP. While acetonitrile and water did not remove (**1**) from NIP, and nearly quantitative amount of (**1**) was found in eluate, the other solvents reduced non-specific adsorption. The trend of suppression could be related with decreasing polarity of the washing phase and the highest reduction was observed for the solution of formamide–methanol 10:90 v/v.

In order to verify the ability of washing solvents to remove only non-specifically bound **(1)**, four solvent characterized by the highest reduction capability on NIP were applied on MIP. The results are presented in Table 2 (right column).

The elution recovery of (**1**) from MIP after washing step with solutions of formamide–methanol 10:90 v/v and formamide–water 10:90 v/v was very low. The results revealed that methanol–water 85:15 v/v and methanol are the optimal for washing step, because the recovery values are close to 100%. We selected methanol–water 85:15 v/v as the washing solvent for further experiments.

3.4.3. Optimization of eluent

In order to optimize the elution step we analyzed the amounts of ammonium acetate as well as the amounts of methanol in eluent. The cartridges filled with MIP were loaded with the standard solution of **(1)** (50 μmol L^{-1}) in methanol–water 85:15 v/v and washed with methanol–water 85:15 v/v. Then the recovery of (**1**) defined as the percentage of adsorbed amount was determined. The following solutions were investigated as the eluents: 0.2 M aq. ammonium acetate–methanol 70:30 v/v, 0.04 M aq. ammonium acetate–methanol 70:30 v/v, 0.008 M aq. ammonium acetate–methanol 70:30 v/v, 0.04 M aq. ammonium acetate–methanol 50:50 v/v, and methanol. The results revealed that the amount of ammonium acetate has the modest impact on the desorption and the recoveries of (**1**) after elution with 0.2 M, 0.04 M, and 0.008 M aq. ammonium acetate–methanol 70:30 v/v were: 98 ± 2%, 98 ± 2%, and 95 ± 2%, respectively. The impact of the methanol in the eluent was significant for the desorption of (**1**). The recoveries of (**1**) after applying of methanol, 0.04 M aq. ammonium acetate–methanol 50:50 v/v, and 0.04 M aq. ammonium acetate–methanol 70:30 v/v were: 38 ± 1%, 94 ± 2%, and 98 ± 2%, respectively. The results proved that the presence of ammonium acetate in the eluent is compulsory for the efficient elution step. We selected 0.04 M aq. ammonium acetate–methanol 70:30 v/v as the eluent for SPE of (**1**).

3.4.4. Optimization of volume of loading solution and mass of imprinted particles

Next, we optimized the volume of loading solution and the mass of particles because both parameters play critical role in SPE and both affected the total recovery of the analyte.

We measured the total recovery of (**1**) from MIP. The loading of the standard solution of **(1)** (50 μmol L^{-1}) on the polymer was performed in SPE mode and only one portion of the standard solution volume of 2, 5, 10, 15, 20, and 30 mL was loaded. Additionally, we used cartridges filled with different mass of MIP, *viz*. 25 and 50 mg. The total elution recoveries (expressed as the percentage of amount of (**1**) in standard solution) are presented in Table 3.

The results revealed that both, the volume of standard solution of (**1**) and the mass of particles affected the adsorption and desorption process. While for the mass of 25 mg of MIP the applying volume of loading solution was relatively low and was equal to 2 mL, for the mass of 50 mg of MIP this parameter was significantly improved. MIP was capable to quantitatively elute (**1**) from 10 mL of loading solution. Higher volumes caused decrease of adsorbed amount and affected the total recovery. We can supposed that the binding capacity of MIP has been exceeded. The mass of 50 mg of MIP and the volumes up to 10 mL of the standard solution of (**1**) were selected as the most effective ones.

3.5. Affinity test

In order to confirm the selectivity of MIP, the binding capacities were determined for five biogennic compounds, *viz*. tryptamine (**2**), serotonin (**3**), octopamine (**4**), synephrine (**5**), and L-tyrosine **(6)** on MIP and NIP by the dynamic procedure using the optimized solvents (see Section 3.4 and Table 4) and the respective affinity factors (AF) were calculated. The dynamic binding procedure was

Table 3
Impact of volume of loading solution combined with impact of mass of the particles on total elution recovery of tyramine (**1**) (conc. 50 μmol L^{-1}, $n=3$).

Mass of imprinted polymer (mg)	Volume of standard solution (mL)	Total elution recovery ± R.S.D. (%)
25	2	105 ± 8
	5	93 ± 7
	10	55 ± 4
	15	33 ± 3
50	5	92 ± 7
	10	96 ± 7
	20	62 ± 5
	30	34 ± 3

Table 4
Binding capacities, affinity factors (AF) and binding energies (ΔE_B) of biogenic compounds (conc. 20 μmol L^{-1}, $n=3$).

Compound	Binding capacity ± S.D. (μmol g^{-1})		AF	ΔE_B (kcal mol^{-1})
	MIP	NIP		
Tyramine (**1**)	7.3 ± 0.4	1.7 ± 0.3	4.27	−27.87
Tryptamine (**2**)	13.0 ± 0.6	3.6 ± 0.6	3.61	−22.11
Serotonin (**3**)	7.1 ± 0.7	2.2 ± 0.4	3.31	−14.89
Octopamine (**4**)	5.5 ± 0.8	1.9 ± 0.3	2.94	−13.27
Synephrine (**5**)	5.9 ± 0.2	2.9 ± 0.3	2.08	−5.15
L-Tyrosine (**6**)	0.11 ± 0.05	0.10 ± 0.03	1.11	−0.18

carried out because it is very similar to loading step of SPE. The low concentration (20 μmol L^{-1}) of standard solution of each biogenic compound was applied. Such concentration allowed to ensure that the selective adsorption of the tested analytes was preferred. Moreover, the adsorption in high affinity binding sites allowed for the appropriate comparison of the experimental results with the theoretical analysis. The binding experiments were performed as the non-competitive ones for the same reason, because in the theoretical investigations the affinity of each single biogenic compound to the polymer was analyzed. Table 4 presents the results for the target analyte (**1**) and for the compounds (**2**)–(**6**). The highest affinity was observed for (**1**) and the binding capacity was also sufficient. The highest binding capacity on MIP was revealed for (**2**), but it was also highest on NIP and as the result the affinity factor was lower than for (**1**). The lowest binding capacity and the lowest affinity factor were determined for (**6**). To interpret these results we used the theoretical model of adsorption inside the polymer cavity.

3.6. MIP affinity – the answer from theoretical studies

The optimized structures of the cavity with the analytes inside are presented in Fig. 6 (for the cavity the molecular electrostatic potential was presented). The figures illustrate the location of the tested compounds at the end of the adsorption process. Next to the cavity, the analytes colored according to the partial charge values, are presented for comparison. The experimental binding capacities and the affinity factors are shown in Table 4. All of the compounds had positive charges located on the H atoms of NH_2 or NH_3^+ groups. These atoms created hydrogen bonds and electrostatically interacted with the functional monomer and the cross-linker molecules (see Fig. 6). Length of all analyzed hydrogen bonds ranged from 1.86 to 2.96 Å. The compounds (**2**)–(**6**) were located inside the cavity similarly as (**1**) but their interactions were weaker. Compound (**1**) created nine hydrogen bonds with the monomer and the cross-linker molecules as was written in Section 3.2. Compound (**2**) formed six hydrogen bonds through N atoms with the polymer cavity (five created by amino group and one formed by N atom from indole ring). Compound (**3**) similarly to (**1**) created nine hydrogen bonds with the monomer and the cross-linker molecules (seven of them were produced by NH_3^+ group and two by OH group). Length of the hydrogen bonds formed between the monomers and (**3**) were longer (2.37–2.75 Å) than those created by (**1**) what resulted in the weaker interactions with the cavity and the lower affinity to MIP. However (**2**) formed less hydrogen bonds than (**1**) and (**3**), its interaction with the polymer matrix was stronger because the absolute value of the charges located on N and H atoms of the NH_2 group was higher than in (**1**) and (**3**), so the electrostatic interactions were stronger. This fact could explain the highest binding capacities of **(3)** on MIP and NIP polymer matrices. Molecule (**4**) interacted with the cavity creating nine hydrogen bonds (six of them was produced by NH_3^+ group, and three by both OH groups). Although it produced the same number of hydrogen bonds as (**1**), we could see that the charges located on NH_3^+ group were lower than in (**1**), (**2**) and (**3**), so the electrostatic interactions were weaker. Compound (**5**) created only four hydrogen bonds with the polymer matrix (two of them were produced by $NHCH_3$ and two by both OH groups) length of 1.86, 2.49, 1,94, 2.08 Å respectively. Moreover, the presence of the CH_3 group connected with N atom caused that the charge distribution on (**5**) is less polarized than on other compounds, and therefore it interacted weaker with the cavity. Its binding capacity was low and non-specific. Furthermore, the bulk methyl group is the steric hindrance to the formation of the intermolecular interactions. Compound (**6**) created six hydrogen bonds (two by NH_2 group, two by COOH group, and two by OH group) length of 2.11, 2.65, 1.88, 2.42, 2.07, 2.70 Å respectively. The acidic COOH group allowed for the formation of hydrogen bonds with COOH groups of the monomer but at the same time limited the formation of the interaction of an adjacent amino group. The charge distribution on (**6**) was also unfavorable, and the interaction of (**6**) with the polymer matrix was the weakest in the set of the tested compounds.

Next, we compared the theoretical energy of binding ΔE_B for all tested molecules (**1**)–(**6**) with the affinity factors. The corresponding energies and the affinity factors are presented in Table 4. The results showed a good correlation between the theoretical binding energy ΔE_B and the experimentally obtained affinity factors. The strongest interaction with MIP was predicted for (**1**) $\Delta E_B = -27.87$ kcal mol^{-1} and the experimentally received affinity factor was the highest also for (**1**) (AF=4.27). The binding energies computed for the tested biogenic compounds (**2**)–(**6**) showed the decrease in strength accordingly to the decrease of affinity factor: (**2**) > (**3**) > (**4**) > (**5**) > (**6**). The aminoacid (**6**) interacted very poorly with MIP ($\Delta E_B = -0.18$ kcal mol^{-1}), and showed practically no affinity to the polymer matrix. This could be summarized as following: the higher binding energy between the analyte and the cavity, the more specific interaction, and the higher affinity factor.

3.7. Solid phase extraction of tyramine (*1*) from bovine serum albumin

To investigate the applicability of MIP to separate (**1**) from the complex samples, spiked bovine serum albumin was used (see Section 2.1.7). The ability of MIP to the effective separation of (**1**) was compared with the extraction capabilities of NIP, as well as with the commercial C18 sorbent employing the optimized SPE protocol for all sorbents. Table 5 presents the results obtained in each step of SPE procedure.

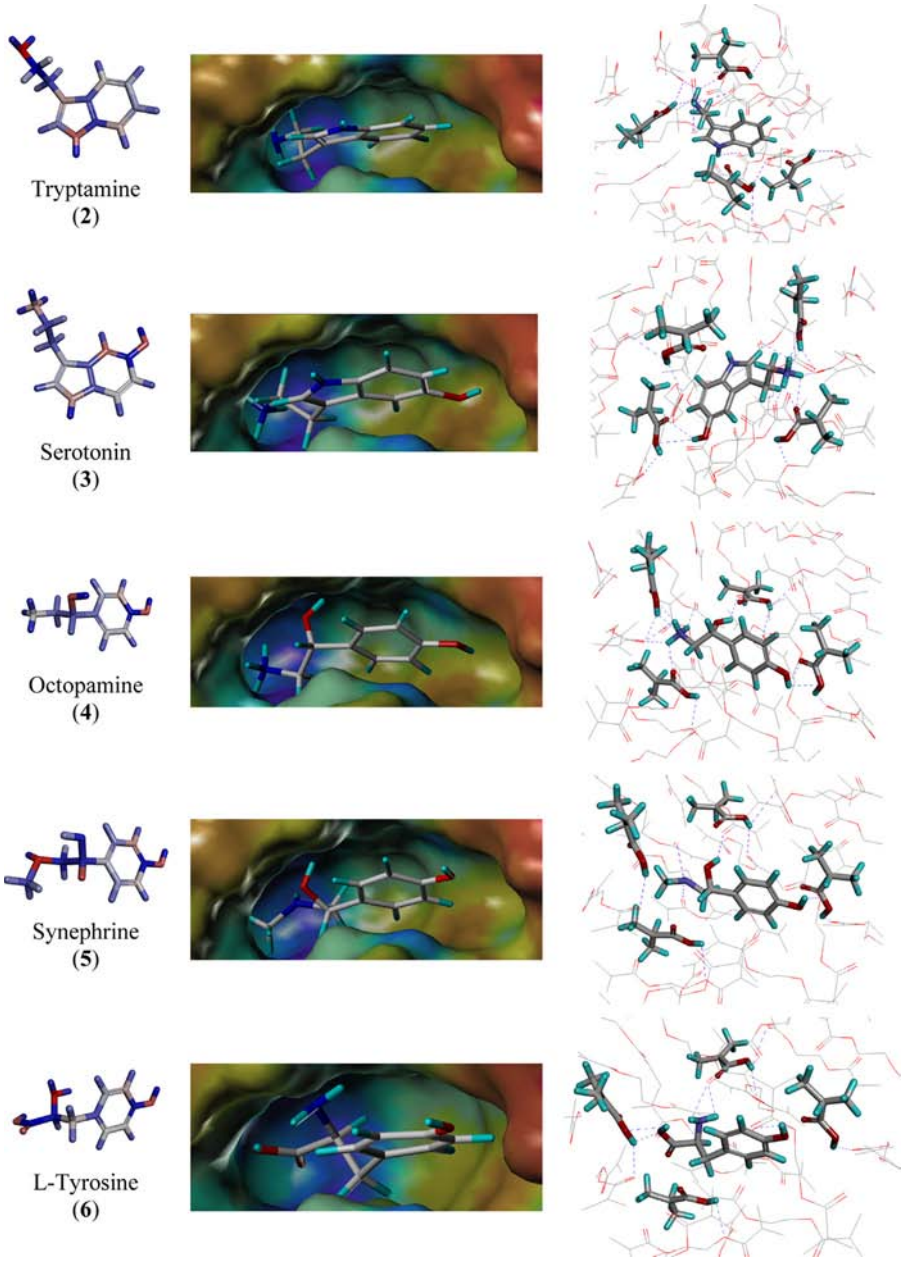

Fig. 6. A view of the analytes at the end of adsorption process. The cavity surface is colored according to molecular electrostatic potential (MEP). Negative values are shown as blue, neutral values – as yellow-green, and positive values – as red-orange. The analytes on the left column are colored according to the partial charge values (negative values are shown as red and positive values as blue). On the right column the hydrogen bonds formed in the polymer cavity are shown as the dashed blue lines. (For interpretation of the references to color in this figure legend, the reader is referred to the web version of this article.)

The C18 sorbent bound only small amount of (**1**), which was washed out completely in the washing step. The particles of NIP had higher binding affinity than C18 towards (**1**), but the recovery was only $14 \pm 3\%$. Only MIP particles have bound (**1**) almost quantitatively and the recovery obtained was equal to $95 \pm 2\%$. These results suggested that the selective extraction and separation of **(1)** was achieved from the solution of the bovine serum albumin, and that MIP was identified as suitable sorbent of **(1)** from the complex samples.

4. Conclusions

The 2-(4-methoxyphenyl)ethylamine imprinted polymer (MIP) was successfully applied as very efficient sorbent for solid phase extraction of tyramine. Binding characteristic of MIP showed two populations of binding sites towards tyramine with $K_d(1) = 9.24\ \mu mol\ L^{-1}$ and $B_{max}(1) = 6.9\ \mu mol\ g^{-1}$ for the higher affinity binding sites, and $K_d(2) = 120\ \mu mol\ L^{-1}$ and $B_{max}(2) = 42.3\ \mu mol\ g^{-1}$ for the lower affinity binding sites. The computational investigations suggested that MIP can be the selective sorbent of tyramine, because of the high binding energy revealing for tyramine, $\Delta E_B = -27.87\ kcal\ mol^{-1}$. The solid phase extraction analysis optimized towards tyramine confirmed the theoretical predictions – the affinity factor for tyramine was equal to 4.27. The theoretical insight on the intermolecular interactions in the polymer cavity model allowed for the evaluation of the binding properties of MIP. The theoretical binding energies of the analytes were the good measure of the selectivity of the polymer matrix towards six analytes: tyramine, tryptamine, serotonin,

Table 5
Separation of tyramine (**1**) in SPE procedure from spiked bovine serum albumin (conc. 52.3 μmol L^{-1}) on MIP, NIP and C18 ($n=5$).

Steps of extraction[a]	Amount of tyramine (nmol)		
	MIP	NIP	C18
Loading, 5 mL of spiked bovine serum albumin	Bound		
	259 ± 4	67 ± 14	22 ± 2
Washing, 1 mL, methanol–water 85:15 v/v	Found		
	2.5 ± 0.8	15 ± 3	14 ± 3
Eluting, 5 mL of 0.04 M aq. ammonium acetate–methanol 70:30 v/v	Found		
	249 ± 4	37 ± 8	5 ± 1
Total recovery (%)	95 ± 2	14 ± 3	1.9 ± 0.4

[a] Conditioning step was carried out and the amounts of tyramine were below LOQ.

octopamine, synephrine, and L-tyrosine. High total recovery of 95 ± 2% of tyramine from MIP noted after SPE protocol from spiked bovine serum albumin and low total recovery from C18 confirmed applicability of imprinted material as efficient sorbent for tyramine.

Acknowledgment

Authors would like to thank Dr Magdalena Bamburowicz-Klimkowska for her assistance in HPLC analysis.

The computational results presented in this work were obtained using the resources of Interdisciplinary Center for Mathematical and Computational Modelling (ICM) University of Warsaw (G26-10).

References

[1] S.A. Burchett, T.P. Hicks, Prog. Neurobiol. 79 (2006) 223–246.
[2] A.B. Lange, Gen. Comp. Endocrinol. 162 (2009) 18–26.
[3] G. D'Andrea, G. Nordera, G. Pizzolato, A. Bolner, D. Colavito, R. Flaibani, A. Leon, Neurosci. Lett. 469 (2010) 348–351.
[4] Z. Xie, G.M. Miller, Biochem. Pharmacol. 78 (2009) 1095–1104.
[5] R. Branicky, W.R. Schafer, Neuron 62 (2009) 458–460.
[6] K.J. Broadley, Pharmacol. Ther. 125 (2010) 363–375.
[7] T. Komprda, R. Burdychova, V. Dohnal, O. Cwikova, H. Sladkova, H. Dvorackova, Food Microbiol. 25 (2008) 219–227.
[8] V. Ladero, N. Martinez, M.C. Martin, M. Fernandez, M.A. Alvarez, Food Res. Int. 43 (2010) 289–295.
[9] M. Yigit, L. Ersoy, J. Pharm. Biomed. Anal. 31 (2003) 1223–1228.
[10] E. Dadakova, M. Krizek, T. Pelikanova, Food Chem. 116 (2009) 365–370.
[11] R. Khwanchuea, M.J. Mulvany, C. Jansakul, Eur. J. Pharmacol. 579 (2008) 308–317.
[12] A. Pena-Gallego, P. Hernandez-Orte, J. Cacho, V. Ferreira, J. Chromatogr. A 1216 (2009) 3398–3401.
[13] V. Gianotti, U. Chiuminatto, E. Mazzucco, F. Gosetti, M. Bottaro, P. Frascarolo, M.C. Gennaro, J. Chromatogr. A 1185 (2008) 296–300.
[14] M. Saaid, B. Saad, A.S.M. Ali, M.I. Saleh, C. Basheer, H.K. Lee, J. Chromatogr. A 1216 (2009) 5165–5170.
[15] D. Djozan, M.A. Farajzadeh, S.M. Sorouraddin, T. Baheri, J. Chromatogr. A 1248 (2012) 24–31.
[16] S. Piletsky, A. Turner, Molecular Imprinting of Polymers, Landes-Bioscience, Georgetown, 2006.
[17] J. Huang, X. Xing, X. Zhang, X. He, Q. Lin, W. Lian, H. Zhu, Food Res. Int. 44 (2011) 276–281.
[18] N.F. Atta, A.M. Abdel-Mageed, Talanta 80 (2009) 511–518.
[19] N.F. Atta, M.M. Hamed, A.M. Abdel-Mageed, Anal. Chim. Acta 667 (2010) 63–70.
[20] T. Żołek, P. Luliński, D. Maciejewska, Anal. Chim. Acta 693 (2011) 121–129.
[21] P. Luliński, D. Maciejewska, J. Sep. Sci. 35 (2012) 1050–1057.
[22] P. Luliński, D. Maciejewska, Mater. Sci. Eng. C 31 (2011) 281–289.
[23] P. Luliński, D. Maciejewska, Mater. Sci. Eng. C 33 (2013) 1162–1169.
[24] M. Sobiech, T. Żołek, P. Luliński, D. Maciejewska, Analyst 139 (2014) 1779–1788.
[25] Accelrys Software Inc., Discovery Studio Modeling Environment, Release 3.1, Accelrys Software Inc., San Diego, 2011.
[26] M.J. Frish, G.W. Trucks, H.B. Schlegel, G.E. Scuseria, M.A. Robb, J.R. Cheeseman, V.G. Zakrzewski, J.A.J. Montgomery, R.E. Stratmann, J.C. Burant, S. Dapprich, J.M. Millam, A.D. Daniels, K.N. Kudin, M.C. Strain, O. Farkas, J. Tomasi, V. Barone, M. Cossi, R. Cammi, B. Mennucci, C. Pomelli, C. Adamo, S. Clifford, J. Ochterski, G.A. Petersson, P.Y. Ayala, Q. Cui, K. Morokuma, D.K. Malick, A.D. Rabuck, K. RaghavachariK, J.B. Foresman, J. Cioslowski, J.V. Ortiz, A.G. Baboul, B.B. Stefanov, G. Liu, A. Liashenko, P. Piskorz, I. Komaromi, R. Gomperts, R.L. Martin, D.J. Fox, T. Keith, M.A. Al-Laham, C.Y. Peng, A. Nanayakkara, C. Gonzalez, M.P. Challacombe, P.M.W. Gill, B. Johnson, W. Chen, M.W. Wong, J.L. Andres, C. Gonzalez, M. Head-Gordon, E.S. Replogle, J.A. Pople, Gaussian 09, Gaussian, Inc., Pittsburgh PA, 2009.
[27] C.M. Breneman, K.B. Wiberg, J. Comput. Chem. 11 (1990) 361–373.
[28] B. Roux, T. Simonson, Biophys. Chem. 78 (1999) 1–20.
[29] M. Cossi, V. Barone, R. Cammi, J. Tomasi, J. Chem. Phys. Lett. (1990) 327–335.
[30] D.R. Lide, Handbook of Chemistry and Physics, seventy first ed., CRC Press, Boca Raton (1990) 9–11.
[31] B.R. Brooks, C.L. Brooks III, A.D. Mackerell Jr, L. Nilsson, R.J. Petrella, B. Roux, Y. Won, G. Archontis, C. Bartels, S. Boresch, A. Caflisch, L. Caves, Q. Cui, A.R. Dinner, M. Feig, S. Fischer, J. Gao, J.M. Hodoscek, W. Im, K. Kuczera, T. Lazaridis, J. Ma, V. Ovchinnikov, E. Paci, R.W. Pastor, C.B. Post, J.Z. Pu, M. Schaefer, B. Tidor, R.M. Venable, H.L. Woodcock, X. Wu, W. Yang, D.M. York, M. Karplus, J. Comput. Chem. 30 (2009) 1545–1614.
[32] B. Kvamme, Phys. Chem. Chem. Phys. (PCCP) 4 (2002) 942–948.
[33] X. Li, S.M. Husson, Biosens. Bioelectron. 22 (2006) 336–348.
[34] Y. Dineiro, M.I. Menendez, M.C. Blanco-Lopez, M.J. Lobo-Castanon, A.J. Miranda-Ordieres, P. Tunon-Blanco, Biosens. Bioelectron. 22 (2006) 364–371.